CAMBRIDGE
UNIVERSITY PRESS

RESEARCH ARTICLE

Fossil and present-day stromatolite ooids contain a meteoritic polymer of glycine and iron

Julie E.M. McGeoch[1,2] (iD), Anton J. Frommelt[3], Robin L. Owen[4] (iD), Gianfelice Cinque[4] (iD), Arthur McClelland[5] (iD), David Lageson[6] and Malcolm W. McGeoch[7] (iD)

[1]Department of Molecular and Cellular Biology, Harvard University, 52 Oxford St., Cambridge, MA 02138, USA
[2]High Energy Physics Div, Smithsonian Astrophysical Observatory Center for Astrophysics Harvard & Smithsonian, 60 Garden St, Cambridge, MA 02138, USA
[3]LRL-CAT, Eli Lilly and Company, Advanced Photon Source, Argonne National Laboratory, 9700 S. Cass Avenue, Lemont, IL, 60439, USA
[4]Diamond Light Source, Harwell Science and Innovation Campus, Didcot, OX11 0DE, UK
[5]Center for Nanoscale Systems, Harvard University, 11 Oxford St, LISE G40, Cambridge, MA 02138, USA
[6]Department of Earth Sciences, Montana State University, 226 Traphagen Hall, P.O. Box 173480, Bozeman, MT 59717, USA
[7]PLEX Corporation, 275 Martine St., Suite 100, Fall River, MA 02723, USA
Corresponding author: Julie E.M. McGeoch; Email: Julie.mcgeoch@cfa.harvard.edu

Abstract

Hemoglycin, a space polymer of glycine and iron, has been identified in the carbonaceous chondritic meteorites Allende, Acfer 086, Kaba, Sutter's Mill and Orgueil. Its core form has a mass of 1494 Da and is basically an anti-parallel pair of polyglycine strands linked at each end by an iron atom. The polymer forms two- and three- dimensional lattices with an inter-vertex distance of 4.9 nm. Here the extraction technique for meteorites is applied to a 2.1 Gya fossil stromatolite to reveal the presence of hemoglycin by mass spectrometry. Intact ooids from a recent (3000 Ya) stromatolite exhibited the same visible hemoglycin fluorescence in response to x-rays as an intact crystal from the Orgueil meteorite. X-ray analysis confirmed the existence in ooids of an internal three-dimensional lattice of 4.9 nm inter-vertex spacing, matching the spacing of lattices in meteoritic crystals. FTIR measurements of acid-treated ooid and a Sutter's Mill meteoritic crystal both show the presence, via the splitting of the Amide I band, of an extended anti-parallel beta sheet structure. It seems probable that the copious in-fall of carbonaceous meteoritic material, from Archaean times onward, has left traces of hemoglycin in sedimentary carbonates and potentially has influenced ooid formation.

Contents

Introduction

Hemoglycin (McGeoch and McGeoch 2015, 2021, 2022; McGeoch *et al.*, 2021) is a polymer of glycine, containing iron, that has been identified in extracts of five carbonaceous chondritic meteorites of primitive types that do not have extensive aqueous or thermal alteration. Having developed effective extraction and analysis techniques for these 'stony' meteorites, we have applied them to first, a 2.1 Gya fossil stromatolite, then to ooids of present-day stromatolite, to ask whether any trace of the compound could have reached the early Earth via in-fall and in some way interacted with biological systems. Two main properties that hemoglycin could contribute are its ability to form open lattices that can accrete materials, and the possibility that it could drive chemical processes via its newly discovered visible absorption band at 480 nm. For background we present in Section S1 a short review of the current state of knowledge on hemoglycin's structure.

In this paper we employed four different experimental approaches in our comparison of stromatolite and meteoritic molecules: mass spectrometry (MS); X-ray induced visible fluorescence; X-ray diffraction, and Fourier transform infrared (FTIR) absorbance. Each of them contributed to the conclusion that the meteoritic polymer hemoglycin was present in stromatolites, ancient and modern. New data emerged on the polymer in meteorites as well as in stromatolites, in particular relating to the secondary beta sheet structure adopted by hemoglycin in at least one meteoritic crystal.

Ooids, the primary mineral component of present-day stromatolites, are small ovoid particles (Fig. 1) of mainly calcium carbonate that make up the oolitic sand that underlies and often overlays

Figure 1. *Shark Bay stromatolite sample with drill hole (left) and Ooids (right) released from the sample by gentle etching. Ooid size range (39 yellow ooids): Major ooid axis 199 ± 42 µm; Waist diameter 164 ± 39 µm.*

their formations. Fossil stromatolites have few intact ooids probably due to pressure over thousands to billions of years since their initial formation. Ooids in present day stromatolites contain calcium carbonate in the aragonite form, but over geological time there can be a transition within ooids to the calcite form, which is more energetically favoured. The formation of ooids, and whether they form during stromatolite growth, or are merely pre-existing entities accreted into stromatolites, is still being researched (Dupraz *et al*., 2009; Trower *et al*., 2018; Diaz and Eberli, 2019; Stolz, 2023). It is considered (Dupraz *et al*., 2009) that there is precipitation of calcium carbonate within stromatolite microbial mats via a matrix of extracellular polymeric substances, firstly in a calcium carbonate gel followed by production of nanospheres and then the growth of aragonite crystals guided by an organic matrix. On the other hand, Trower *et al*. (2018) have documented independent ooid growth that is faster in a turbulent shallow water shoal (Turks and Caicos Islands) than in a more static lagoon with more extensive biofilm colonization. There is extensive evidence for organics within biologically produced aragonite, coming from (a) crystal anisotropy (Berman *et al*., 1993; Pokroy *et al*., 2004) and (b) the presence in ooids of a blue fluorescence (Dravis and Yurewicz, 1985; Paterson *et al*., 2008; Lin *et al*., 2022). In regard to (b), Lin *et al*. (2022) analysed Holocene ooids (5377 ± 61 Ya) from oolitic sand in the Western Qaidan Basin, Tibet. These were well-preserved, lacked microbial evidence, and contained 90–97% aragonite in fine crystals. The blue fluorescence under 365 nm UV light was attributed to organic material within or between the crystals. In a study of present-day stromatolites on Highborne Cay, Exuma, Bahamas, Paterson *et al*. (2008) reported blue fluorescence of ooids under 405 nm light, referring to it as 'autofluorescence' to distinguish it from marker fluorescence. Elsewhere, Dravis and Yurewicz (1985) reported strong fluorescence of ooids within a Pleistocene oolitic grainstone from West Caicos Island. The fluorescence was bright in well-preserved aragonite grains but freshwater diagenesis, that replaces aragonite with more stable calcite, apparently destroyed organic material and removed the fluorescence. These reports did not give fluorescence spectra in sufficient detail to allow comparison with the present X-ray induced visible fluorescence from ooids. A comparison of this fluorescence in meteorites (McGeoch *et al*., 2023a) and ooids from a recent Shark Bay, Australia stromatolite, is presented below in Section 2 of this paper.

In prior work on crystals of meteoritic hemoglycin we had observed two-dimensional lattices via the strong X-ray scattering of iron atoms at the lattice vertices, which are spaced by a hemoglycin polymer of length of 4.9 nm. In (McGeoch and McGeoch, 2021) a floating three-dimensional lattice was reported in the interphase region of the solvent extraction vial, and its structure was proposed to be the diamond 2H form. Subsequently, the tetrahedral angles of this form were seen in X-ray diffraction, but information was partial. In the present work we used light at 2.066 Angstroms, longer than the iron K absorption edge, to reveal the nature of this lattice in present day ooids, data presented in Section 3 below.

The hemoglycin core unit (McGeoch *et al*., 2021; McGeoch and McGeoch, 2022) contains two antiparallel strands in a two-strand beta sheet. Infrared absorption data, discussed in Section 4 of this paper shows, in both a meteoritic crystal and an extract of a recent stromatolite ooid, the characteristic splitting of the Amide I poly-peptide band in the region of 6 microns that is only present in extended arrays of antiparallel beta sheets. This implies that in the meteorite crystal the hemoglycin core units are hydrogen-bonded edge-to-edge in an extended sheet (Fig. S1.2), with the same being true for the structural protein in ooids, data presented in Section 4 of this paper.

In summary, mass spectrometry, X-ray induced visible fluorescence, X-ray diffraction and infrared absorption all point to the organic lattice of ooids being a molecule with the optical and spatial properties of meteoritic hemoglycin. The bulk of an ooid, filling this lattice, is a crystalline mixture of aragonite and calcite. In the discussion we assess meteoritic in-fall as the source of this lattice material.

Methods

Sample sources

Present-day stromatolites are supplied by Andrew Knoll of the Museum of Comparative Zoology and Organismic and Evolutionary Biology (OEB) Harvard.

Present-day stromatolite details are:

1. Shark-Bay Western Australia – The sample was collected by Elso Barghoorn in 1971, from Hamlin Pool, Shark Bay, Western Australia. This area is now protected but was not when the sample was collected in 1971. The stromatolites are estimated to be 2000–3000 years old.
2. Sample K-05 SS-1 from San Salvador Island, Bahamas – collected by Knoll (2012) in 2005 – A modern mineralized microbialite.

The Fossil stromatolite samples were collected by David Lageson from the Medicine Bow region, Wyoming craton (Bekker and Eriksson, 2003). The geological history of these rocks was relatively benign with an estimated maximum temperature underground of 300°C, giving hope that molecular information could have survived to the present.

The fossil stromatolite details are as follows:

1. 2.1 Gya stromatolite No. 1 from Medicine Bow region, Wyoming – collected by David Lageson of Montana State University.
2. 2.1 Gya stromatolite No. 2 from Medicine Bow region, Wyoming – collected by David Lageson of Montana State University.

The meteorite details are as follows:

1. The Orgueil meteorite sample was supplied to JEMMc by the Museum National D'Histoire Naturelle, Paris, France (MNHN). Orgueil is a type CI1 carbonaceous chondrite that fell in 1864 in France (Meteoritical Bulletin).
2. Sutter's Mill meteorite (n.d.) sample was supplied to JEMMc by Michael E. Zolensky, NASA. Sutter's Mill is a type C carbonaceous chondrite that fell in California in 2012 (Meteoritical Bulletin).

Mass spectrometry

All experimental procedures were performed under clean laboratory conditions with operators wearing lab coats, hair cover and gloved hands as previously reported (McGeoch and McGeoch, 2015) (Fig. 2) All chemicals were only used for these analyses and kept in separate laboratory areas. Micron particles of the fossil stromatolite were etched as previously described for meteorites and then Folch extracted (McGeoch and McGeoch, 2015, 2022) for up to 5 months at room temperature. The Orgueil meteorite sample being a total of 2×100 mg samples from the Museum National D'Histoire Naturelle (MNHN) with a very loose topology typical of this meteorite, was not etched to micron particles but soft, small pieces of a few mg each were Folch extracted for 4 months.

Crystals of hemoglycin were picked up from the liquid interphase layer of the Folch extraction and pipetted into a watch glass on the stage of a zoom microscope under $\times 25$ magnification. Clean empty Hampton crystallography loops were used to pick up the 100–200 μm crystals. The glycine rods of hemoglycin make the crystals slightly sticky allowing light adhesion to the loop. The Hampton loops were carefully placed into the inside of 500 μl Eppendorf tubes containing 20 μl of methanol. The loops were turned to make sure the crystals were delivered to methanol in the tubes and checked for this under the microscope. Several crystals were added to each Eppendorf tube. This technique of crystal transfer was used for both the fossil stromatolite and the Orgueil crystals. The fossil stromatolite crystals always had some adhering calcium carbonate particles. All stromatolite transfers were performed separate from those for Orgueil transfers to avoid any cross contamination. Each sample of crystals contained at least five separate crystals.
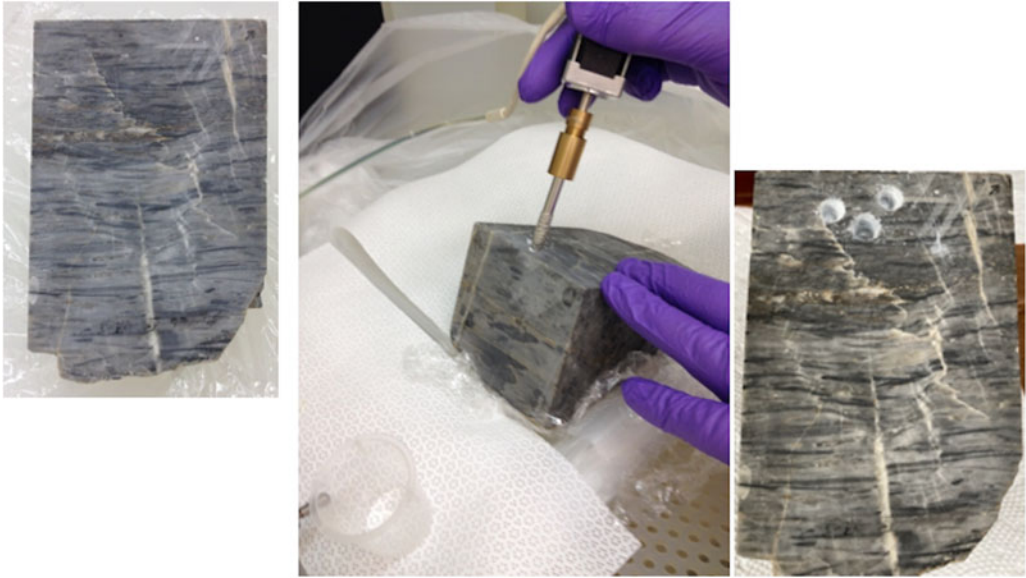
Figure 2. *Etch of the fossil stromatolite to produce micron particles for Folch extract in a clean room. Left, before etch; Middle – the etch using a stepper motor (no brushes to avoid metal contamination) with a vacuum brazed diamond drill bit (to avoid animal origin glue on drill bit); Right – three drill holes are visible. The micron particles are decanted by inversion of the sample over a glass container.*

A separate Orgueil Eppendorf tube was set up from a tube where hemoglycin crystals derived from unprocessed insoluble organic matter (IOM) had dried out and the crystals had adhered to the wall on the inside of the tube to an extensive degree (sample O3_1). Attempts were made using Folch solvents to solubilize these wall crystals which failed. It was decided as those crystals were potentially good because they resembled those that absorbed light (McGeoch and McGeoch, 2022), to simply leave the crystals of O3_1 as is and rely on their solubilization via trifluoroacetic acid (TFA) at the point they are added to the Sinapinic acid matrix (SA) and α-Cyano-4hydroxycinnamic acid matrix (CHCA). After etching, two separate fossil stromatolite Folch extractions of 24 h, were also set up as S3_1 for CHCA matrix and S3_2 for SA matrix. From these, 100 µl aliquots from the interface layer were pipetted into Eppendorf tubes at 24 h of extraction and allowed to reduce in volume to 20 µl by loose cap room temperature evaporation. 2 µl aliquots of each were used for the mass spectrometry analysis with paired CHCA and SA matrices.
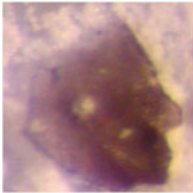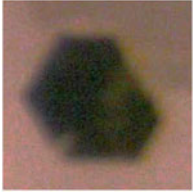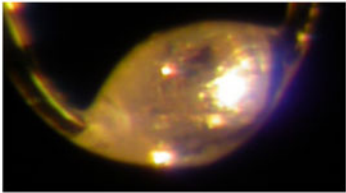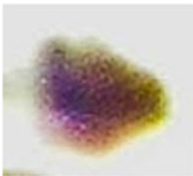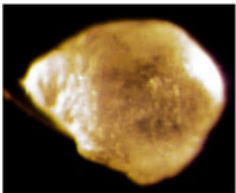
In total there were 11 Matrix Assisted Laser Desorption (MALDI) mass spectrometry analyses performed, shown in Table 1. Throughout, the sample prefix is 'S' for stromatolite and 'O' for Orgueil.:

Mass spectrometry was performed on a Bruker Ultraflextreme MALDI-TOF/TOF instrument. We used CHCA and SA matrices. Both were at $10\,mg\,ml^{-1}$ in 50% acetonitrile in water, 0.1% trifluoroacetic acid in water. Our resolution was of the order of 10 000 and we looked in the range $m/z = 0$–5000, finding most peaks from 750–2000. A sample volume of 2 µl was mixed with a matrix volume of 2 µl, vortexed and left for one hour at room temperature. This one hour wait before pipetting 1 µl quantities onto the MALDI plate is essential as it takes that long to partly solubilize hemoglycin in the matrix solvents.

X-ray induced visible fluorescence of ooids

The Shark Bay recent stromatolite (Fig. 1) was provided by Dr Andrew Knoll. Drilling as above (into fossil stromatolite) did not produce micron particles in recent stromatolite because the material was

Table 1. *Detail of the 11 samples analysed by MALDI mass spectrometry*

Sample source	Tube label	Matrix	Crystal origin
Fossil Stromatolite	S1_1	CHCA	Mauve hexagonal crystals
Fossil Stromatolite	S1_2	SA	Mauve hexagonal crystals
Fossil Stromatolite	S2_1	CHCA	Pale crystals
Fossil Stromatolite	S2_2	SA	Pale crystals
Orgueil meteorite	O1_1	CHCA	Mauve hexagonal crystals
Orgueil meteorite	O1_2	SA	Mauve hexagonal crystals
Orgueil meteorite	O2_1	CHCA	Pale crystals
Orgueil meteorite	O2_2	SA	Pale crystals
Orgueil meteorite	O3_1	CHCA	IOM Folch crystals
Fossil stromatolite	S3_1	CHCA	Folch interphase
Fossil stromatolite	S3_2	SA	Folch interphase

friable, breaking up into 200–500 micron scale fragments, accompanied by intact ooids (Fig. 1). All experimental procedures were performed under clean laboratory conditions with operators wearing lab coats, hair cover and gloved hands as previously reported. All chemicals were only used for these analyses and kept in separate laboratory areas.

Ooids were placed in a watch glass and manipulated under × 25 magnification. Ethyl cyanoacrylate glue (1/5th the volume of the ooid) was applied to a Hampton crystallography loop and the ooid attached to the loop by gently touching the glue to the crystal. After the glue solvents had evaporated (4 h at 18°C) the ooid post and loop assembly was capped, attached to a pad to prevent vibration and was sent by FEDEX to Diamond Light Source. The internal structure of an ooid was obtained by treating ooids in a watch glass with 5% acetic acid. Within 5–10 min the internal vesicular structure was revealed (Fig. 3).

X-ray induced visible fluorescence data were collected at a wavelength of 1.000 Angstroms (12.40 keV) and with a beam size of 50 μm × 50 μm. The flux of the unattenuated beam was 8×10^{12} ph s^{-1} and fluorescence data was collected with the beam attenuations of 2, 5, 10, 20, 40, 60, 80, 100%. UV-Visible data were collected *in situ* using off axis reflective objectives and were recorded over the wavelength range 250–800 nm using an Andor shamrock 303i spectrograph and CCD detector.

X-ray structural analysis

Two X-ray wavelengths, 0.979 Angstroms and 2.066 Angstroms, were used on the APS beamline 31-ID-D. Data were recorded using a Pilatus3 S 6 M detector with a detector distance of 190 mm except where noted, 1 degree oscillations, and exposure times of 0.5 s. On Diamond beamline I24 diffraction data were recorded using a Pilatus3 6 M detector with a detector distance of 300 mm using 0.1° oscillation per frame, exposure times of 10 ms and beam attenuated by 50%.

Infrared absorption spectra

Meteorite sample analysed on beamline B22, Diamond Light Source

A Sutter's Mill crystal (SM2) previously analysed for structure and visible light absorption (McGeoch and McGeoch, 2022) was transferred from beamline I24 to B22 at Diamond Light Source for multimode infrared imaging and micro-spectroscopy. This crystal was kept on its loop for the IR absorption at B22 supported by modelling clay. The crystal was first scanned on its entire area for IR absorption and the amide I and II bands were concentrated in approximately 40 × 20 microns in an ordered
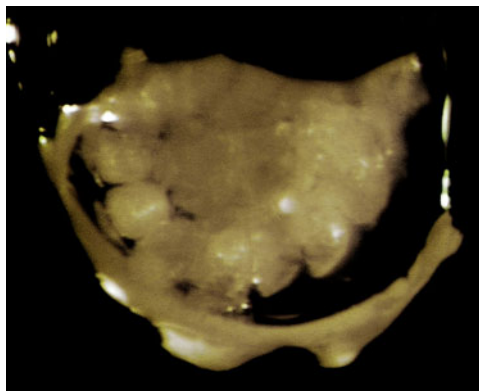

Figure 3. *5% acetic acid treated ooid from present-day stromatolite, Shark Bay, Australia. The ooid (sample LS2) is on a crystallography loop for X-ray diffraction analysis. The individual vesicles revealed via the acid treatment are 20 μm diameter.*

crystalline area near the centre of the loop. Data from this area was collected in detail and compared with surrounding areas. This indicated which bands correlated with amide as opposed to belonging to non-amide content.

Stromatolite Ooid sample analysed at Harvard Center for Nanoscale Systems (CNS MET-15 Bruker FT-IR Lumos 1 Microscope)

Present-day stromatolite ooids were placed under × 25 magnification on glass slides containing carbon tape to stably secure each ooid. X-ray data had revealed these ooids contained principally the aragonite form of calcium carbonate. It was found that this calcium carbonate content dominated the IR absorption spectrum at wavelengths 6.9, 11.7 and 14 microns. Mild acetic acid treatment was applied to reduce this calcium carbonate absorption signal. Ooids secured by carbon tape on glass slide were placed in glass stain containers which contained 5% acetic acid or distilled water. First, for times between 5 min and 1 hour the slides were in the acetic acid followed by washes in 4 separate containers containing distilled water. At the end of this acid treatment regime the slides were air dried and analysed for IR absorption. It was found that 20 min was the ideal time to remove enough calcium carbonate from the ooids to produce a clear IR absorption related to extended antiparallel beta sheets (Amide I at 6 μm). At 20 minutes an amorphous calcium carbonate absorption was also present.

Results

Section 1. Mass spectrometry on fossil stromatolite compared to Orgueil meteorite

Approach

Our decision to employ MALDI mass spectrometry, in this and all our prior analysis was impelled by:

1. Unknown phase mixtures can be handled.
2. A useful degree of laser fragmentation contributes to the structural analysis.
3. There are two stand-out matrix molecules, CHCA and SA, that have reliable, yet very different protonation rates (Lu *et al.*, 2015). When their results coincide, uncertainty is removed.
4. Even when collections of small crystals are studied, as in this work, it is not necessary to grind the crystals as partial solvation is achieved in MALDI matrix solutions after 1 h at room temperature.

We came into the measurements knowing that the Orgueil crystals likely contained hemoglycin because they derive from the interphase of the relevant Folch extractions, where hemoglycin was the dominant chemical (McGeoch *et al.*, 2021). To anticipate the results, we have obtained mass spectrometry confirmation in both Orgueil and fossil stromatolite that the 1494 Da hemoglcyin core unit (McGeoch *et al.*, 2021) comprises essentially 100% of the crystalline material that is able to be solubilized.

Basic observations from mass spectrometry

A very consistent mass spectrometry (MS) pattern was seen in all samples, indicating that the crystal preparation process had universally selected the same molecule, whether from Orgueil or Stromatolite. In every sample the MALDI spectrum contained only two main peaks, one at 1494 *m/z*, corresponding to the hemoglycin 'core unit' (McGeoch *et al.*, 2021) and the second at 760 *m/z*, which was typically five times higher in summed ion count and was the exclusive fragment of 1494 *m/z* observed in the present work. The 760 *m/z* fragment comprises a single polyglycine strand from the antiparallel pair that comprise the central body of hemoglycin. It does not show [54]Fe side peaks (McGeoch *et al.*, 2021) beside the 'monoisotopic' peak, and hence the fragment does not carry iron.

Figure 4 shows for Orgueil crystal sample (O1_2, run 1, SA) the 760 *m/z* peak system on the left, and the 1494 *m/z* system on the right. They were each fitted to a global ^{2}H enhancement, giving via 760
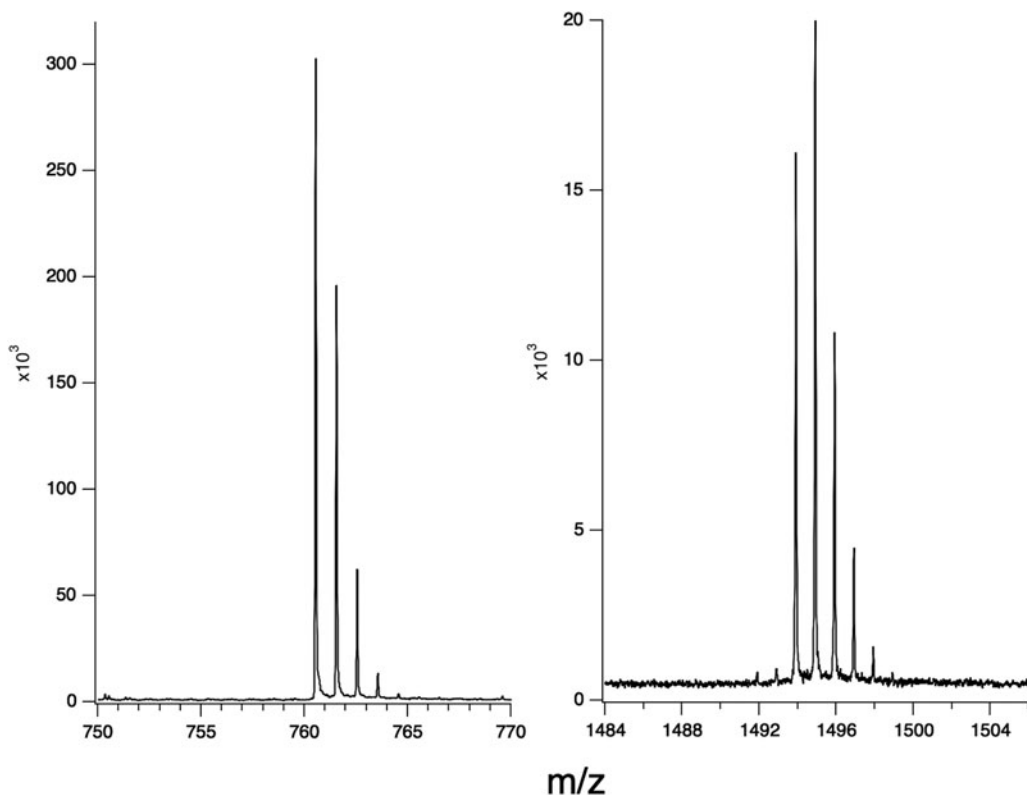
Figure 4. *Data from sample O1_2, with sinapinic acid matrix. On the left is the 760 m/z fragment that is the sole product from the break-up of the 1494 molecules. On the right, the 1494 m/z peak system.*

m/z analysis $\delta\ ^{2}$H = 54 000 ± 3000 per mil, and via the 1494 m/z analysis $\delta\ ^{2}$H = 51 000 ± 3000 per mil. Definitions of 'global' and 'per mil' are given in Section 1.3.

In summary, the strong polymer rod interconnections of hemoglycin rendered MS analysis for the 1494 m/z subunit itself fairly difficult. This was an inevitable side-effect of having a strong space polymer. The difficulty persisted in spite of mixing in MALDI solvent for 1hour ('run 1'), or 72hrs ('run 2', with improved signal-to-noise relative to 'run 1'). Earlier it had been established that 1 h in the matrix with 50% acetonitrile and 0.1%TFA was necessary to get the polymer solvated. Immediate MALDI approximately 15 min after applying to the MALDI plate, yielded no peaks at all with the polymer not leaving the crystals for the matrix.

Isotope analysis

The enrichment of ^{2}H relative to H is defined by the 'per mil' $\delta\ (^{0}/_{00})$ measure:

$$\delta^{2}H(^{0}/_{00}) = \left(\frac{(^{2}H/H)_{SAMPLE}}{(^{2}H/H)_{VIENNA}} - 1\right) \times 1000 \text{ in which } (^{2}H/H)_{VIENNA}$$

$$= 155.76 \pm 0.05 \times 10^{-6} \text{ (IAEA, Vienna, 1995).}$$

Without separate knowledge of ^{15}N enhancement in hemoglycin we fitted the prominent isotope enrichments as if ^{2}H was the only contributor. When ^{15}N values come available the quoted 'global' ^{2}H enrichments may be modified as follows where Δ represents the degree of change:

$\Delta(\delta^2 H) = -7.73\Delta(\delta^{15}N)$. This relationship holds for polymers of glycine and hydroxyglycine that have $N_H/N_N = 3$ and may be scaled via the relationship $R_N N_N/R_H N_H = 7.73$ ($^0/_{00}$) using the R_N and R_H values listed below. The following isotope ratios (IAEA, Vienna, 1995) are taken as terrestrial standards:

VSMOW water	$R_H = {}^2H/{}^1H = 155.76 \pm 0.05 \times 10^{-6}$
VSMOW water	$R_O = {}^{18}O/{}^{16}O = 2005.20 \pm 0.45 \times 10^{-6}$
V-PDB	$R_C = {}^{13}C/{}^{12}C = 11\,237.2 \times 10^{-6}$
Atmospheric Nitrogen	$R_N = {}^{15}N/{}^{14}N = 3612 \pm 7 \times 10^{-6}$

In previous work (McGeoch *et al.*, 2021, 2023b) we concluded that ^{13}C and ^{18}O variations from terrestrial are far less than ^{15}N and ^2H variations in polymer amide from carbonaceous chondrites.

The first identification of hemoglycin in meteorites via MALDI (McGeoch *et al.*, 2021) showed that it carried heavy isotopes ratios such as $^2H/H$, $^{13}C/^{12}C$, $^{15}N/^{14}N$, etc. at levels far above terrestrial standards, at least in the cases of ^2H and ^{15}N. An isotope fitting routine was written (McGeoch *et al.*, 2021) with no internal approximations, in which trial values of the isotope ratios are input and the output is compared to experimental MALDI peak strengths. Figure 5, curve A, shows a stromatolite hemoglycin molecular peak complex at m/z 1494 (sample S2_1 (CHCA)). The highest isotopologue occurs at the $n = +1$ location relative to the $n = (0)$ 'monoisotopic' peak. Curve B in Fig. 5 is the calculated complex for a 'global' (i.e. equivalent ^2H) enhancement of 52 000 per mil, but it is expected that in practice there would be a significant ^{15}N component, as seen in Acfer 086 (McGeoch *et al.*, 2023b). This would reduce the actual $^2H/H$ ratio by the amount discussed above. 'Global ^2H' fitting to the higher signal-to-noise ratio run 2 data set, from both the 1494 and 760 components, is summarized in Table 2. In contrast, a simulation with wholly terrestrial isotope levels gives the very different curve (Fig. 5C), in which the highest peak is the (0) isotopologue.
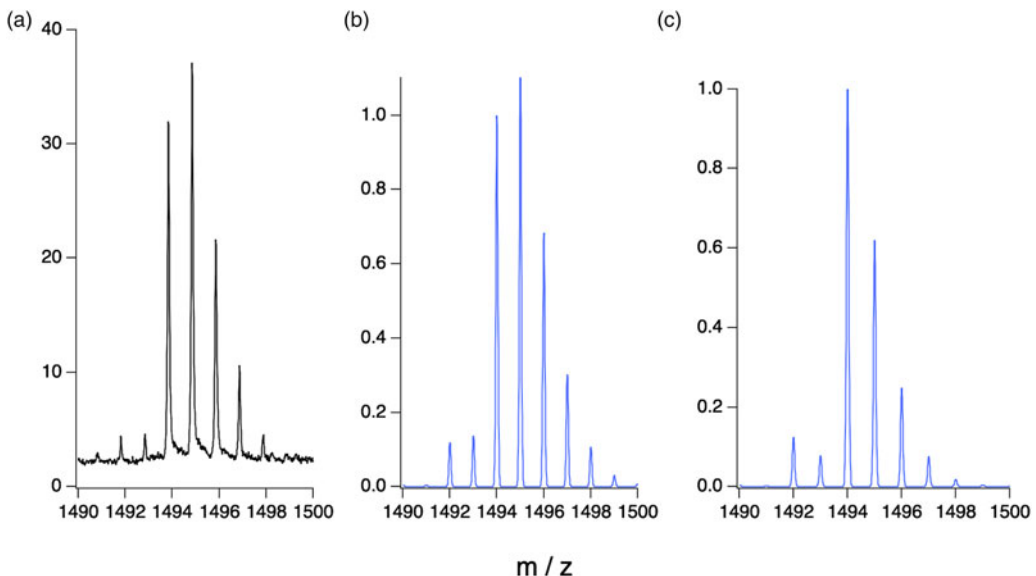

Figure 5. *Vertical axis is intensity (arbitrary units) and horizontal axis m/z. A: sample S2_1 peak complex at 1494 m/z. B: variation of ^2H to fit the isotopologue intensities in curve A (the fit required $\delta\,^2H = 52\,000$ per mil). C: the same molecule simulated at terrestrial (Vienna) isotope values.*

Table 2. *Isotope analysis for run 2 data set*

		Global ^{2}H 760 *m/z*	Global ^{2}H 1494 *m/z*
Orgueil	O1_1 (CHCA)	xx	$55\,000 \pm 2000$
	O1_2 (SA)	xx	$54\,000 \pm 3000$
	O2_1 (CHCA)	$50\,000 \pm 2000$	xx
	O2_2 (SA)	$51\,000 \pm 2000$	xx
	O3_1 (CHCA)	$51\,000 \pm 2000$	$53\,000 \pm 3000$
		Orgueil Ave. 52 333 $\sigma = 1795$ $n = 6$	
Stromatolite	S1_1 (CHCA)	xx	$53\,000 \pm 3000$
	S1_2 (SA)	xx	$53\,000 \pm 3000$
	S2_1 (CHCA)	xx	$52\,000 \pm 3000$
	S2_2 (SA)	xx	$54\,000 \pm 2000$
	S3_1 (CHCA)	xx	$51\,000 \pm 2000$
	S3_2 (SA)	xx	xx
		Stromatolite Ave. 52 600 $\sigma = 1019$ $n = 5$	

Enhancements in parts per mil.
'xx' represents saturated signal or too low signal relative to noise.

Section 2. Visible ooid fluorescence induced by X-rays

An ooid (sample LS2) from Hamlin Pool, Shark Bay, Western Australia of estimated age 2000–3000 years, that had been treated with acetic acid as described in the Methods section to partially remove calcium carbonate, was the subject of x ray analysis at Diamond Light Source. Sample LS2 gave strong X-ray induced fluorescence in a 1.000 Angstrom beam, under cryo-flow cooling (Fig. 6). The fluorescence was associated with low temperatures (100 K) and was absent at 300 K. The fluorescence peaked at 485 nm and carried the same 465 nm absorption 'dip' seen previously in X-ray induced fluorescence (McGeoch *et al*., 2023a) in a crystal from the Orgueil meteorite (n.d.), the data for both cases being shown in Fig. 6.

The fluorescence was analysed as before (McGeoch *et al*., 2023a) using five Gaussian components to obtain an exact comparison. Across the range of wavelengths the same five components appeared, with relatively minor changes to the centre wavelength of any one component. The intensity distribution was different, however, with much reduced representation of the peaks at 500 and 557 nm relative

Table 3. *Peak X-ray induced visible fluorescence wavelengths, half widths at 1/e intensity, and relative integrated strengths, for an Orgueil crystal (McGeoch* et al*., 2023a) and ooid from stromatolite*

Peak	1	2	3	4	5
ORGUEIL, λ (nm)	408.5 ± 0.4	489.0 ± 0.3	551.2 ± 9.7	465.1 ± 0.2	488.5 ± 0.5
1/e half width (nm)	27	72	100	12.0	15.3
Peak intensity	408 ± 16	2826 ± 135	714 ± 98	-759 ± 15	339 ± 10
Integrated strength normalized	5.4	100	35	-4.5	2.5
OOID λ (nm)	407.7 ± 0.6	500.5 ± 4.3	557.2 ± 5.6	464.9 ± 0.1	477.7 ± 0.5
1/e half width (nm)	39	79	166	12.7	37
Peak intensity	3563 ± 218	3678 ± 218	496 ± 42	-1940 ± 29	3028 ± 251
Integrated strength normalized	48	100	28	-8.5	38

Errors were generated in least squares fitting of averages of 3 data traces taken at 100% beam intensity. Peak 4 is the absorption dip, represented by a negative intensity
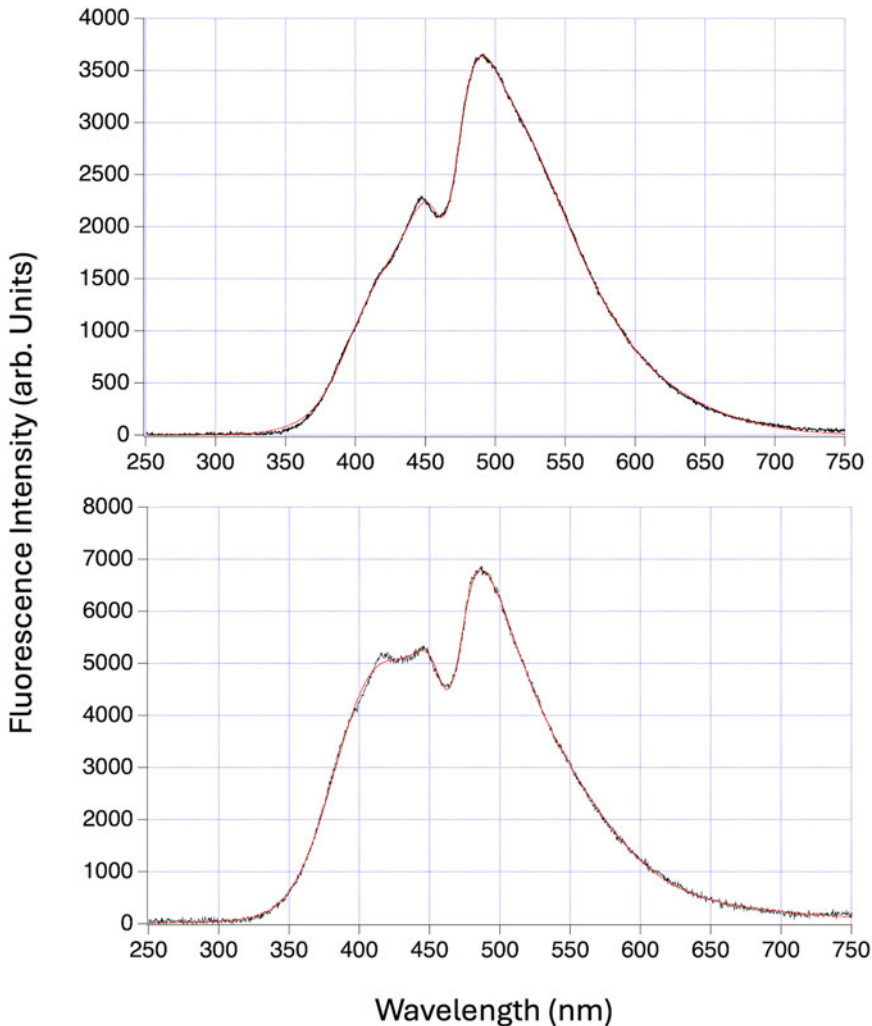
Figure 6. *X-ray induced blue-green fluorescence from (Top) Orgueil meteorite crystal; (Bottom) Ooid from present day Shark Bay Stromatolite. Experimental data black, fit curves in red.*

to the corresponding ones in the Orgueil data at 489 and 551 nm. These distributions are compared in Table 3. Intensities are multiplied by widths and normalized to the 489 nm Orgueil peak, which is assigned the value 100. The Orgueil bands at 489 and 551 nm were previously seen to track together, and it was conjectured (McGeoch *et al.*, 2023a) that they shared a common upper level that also was the upper level of the chiral 480 nm absorption (McGeoch and McGeoch, 2022). In ooid this pair (now 500 and 557 nm) still have roughly the same ratio to each other, but now are an order of magnitude lower compared to the ooid pair at 408 and 478 nm which also remain in roughly the same ratio to each other in both samples. All of these emissions are linked to the interaction of iron with glycine residues.

The ultraviolet and visible light absorbance of the sample (not shown) is featureless, not showing the characteristic 480 nm absorbance seen in the Orgueil crystal that is indicative of the chiral 480 nm absorbance of hemoglycin (McGeoch and McGeoch, 2022). This suggests that in the ooid sample there is probably a low population of 'R' chirality hydroxy-glycine residues bonded to Fe at their C-termini. More specifically, reviewing the visible absorptions calculated in Table 2 of McGeoch and McGeoch, 2022) we deduce that there appear to be low populations of {0,R}, {S,0}, {S,R}, {R,0}, {R,S}, {R,R}

combinations of {N-terminus, C terminus} chiralities of hydroxyglycine, with zero representing plain glycine. It is possible that the acetic acid treatment of this sample caused chemical reduction of most of the hydroxyl groups, leading to un-observable 480 nm absorbance, and consequently to a large reduction in the associated fluorescence bands (at 489 and 551 nm) while leaving the other correlated emission band pair (at 408 and 478 nm) unchanged. Calcium ions associated with aragonite in the ooid (Section S3.2) may also be interacting to slightly modify the fluorescence bands, relative to the Orgueil case in which the matrix material could not be identified by x-ray diffraction.

The two fluorescence curves are certainly from the same basic molecule, identified in McGeoch *et al.*, 2023a) as hemoglycin. Focusing on the fitted wavelength components of Table 3 we label the ooid peaks 'test' and the Orgueil peaks 'control'. Forming the quotient (test(nm)-control(nm))/(data range of 143 nm) we have a rough measure of the probability of randomly observing such a match for a given band. The probability of simultaneously obtaining all five matches is then of the order of 10^{-6}, a number dominated by the small probability of the extremely close matches at 408 and 465 nm. Beyond this, only the test band at 465 nm is an absorption, for which, out of five bands, there is an a-priori chance of 1/32 that it should be co-located with the only control absorption. Observation of the sharp 465 nm absorption again in ooids suggests that there could be a 'caged' iron atom at junctions of the ooid hemoglycin lattice, as previously proposed for the Orgueil crystal (McGeoch *et al.*, 2023a).

Section 3. X-ray derivation of the three-dimensional hemoglycin lattice in ooids

As a matter of course the X-ray scattering of present day ooids was recorded, this time at wavelengths above and below the iron K-edge at 1.74 Angstroms so as to potentially know whether iron was involved in the organic internal lattice. At the longer 2.066 Angstrom wavelength used, where iron scattering was high and yet absorption was low, a dramatic series of high order diffraction rings was seen that did not appear at 0.979 Angstroms. Additionally, the anticipated aragonite and calcite rings at low 'd' spacings were present in both cases. An analysis of this ooid data revealed a diamond 2H lattice of vertex spacing 4.9 nm with a small axial lengthening above the ideal geometric lattice, presented in the present section with more detail in Supplementary Section S2.

Intact ooids from the Shark Bay stromatolite sample were studied for lattice structure at APS using X-ray wavelengths of 0.979 Angstroms and 2.066 Angstroms which straddled the 1.74 Angstrom K absorption edge of iron. At each wavelength there were diffraction rings between principally 1.61 Angstroms and 3.85 Angstroms in a superposition of calcite and aragonite powder pattern rings (data in S2, Table S2.1 and Fig. S2.2, part B). However, at 2.066 Angstroms, where Fe absorption is low, and not at 0.979 Angstroms, there was an intense and striking new set of rings (Fig. 7 and Figures S2.1, S2.2) at nominal first order spacings of between 4.808 and 11.540 Angstroms, summarized in Table 4.

The left hand column of Table 4 contains the set of 18 rings that represented larger 'd' spacing than 4 Angstroms. These rings did not match either the calcite or aragonite values but were reminiscent of the ladders of high order diffraction previously seen in hemoglycin lattices (McGeoch and McGeoch, 2021, 2022). In (McGeoch and McGeoch, 2021) the ladder contained orders 2 through 5, with a fitted first order lattice parameter of 48.38 ± 0.2 Angstroms. In (McGeoch and McGeoch, 2022) the ladder contained orders 2 through 12, with a fitted first order parameter of 49.03 ± 0.18 Angstroms. Quick inspection of the present 18 ring set yielded a fit to 49.0 Angstroms in 5th 6th 7th and 9th orders as follows (listed also in Table 4):

$5 \times 9.823 = 49.11$; $6 \times 8.127 = 48.76$; $7 \times 7.022 = 49.15$; $9 \times 5.445 = 49.00$.

Consequently, a complete scan was made to find clusters of orders that matched target 'D' spacing values from 30 Angstroms to 140 Angstroms, rising in increments of 0.05 Angstroms. Results were accumulated whenever a multiple of one of the 18 first order values matched one of these trial 'D' values within less than 0.5% i.e. $D = nd_K$, with $n = 12,3,\ldots$ where the measured first order spacing is $d_K = \lambda/(2\sin\Theta_K)$.
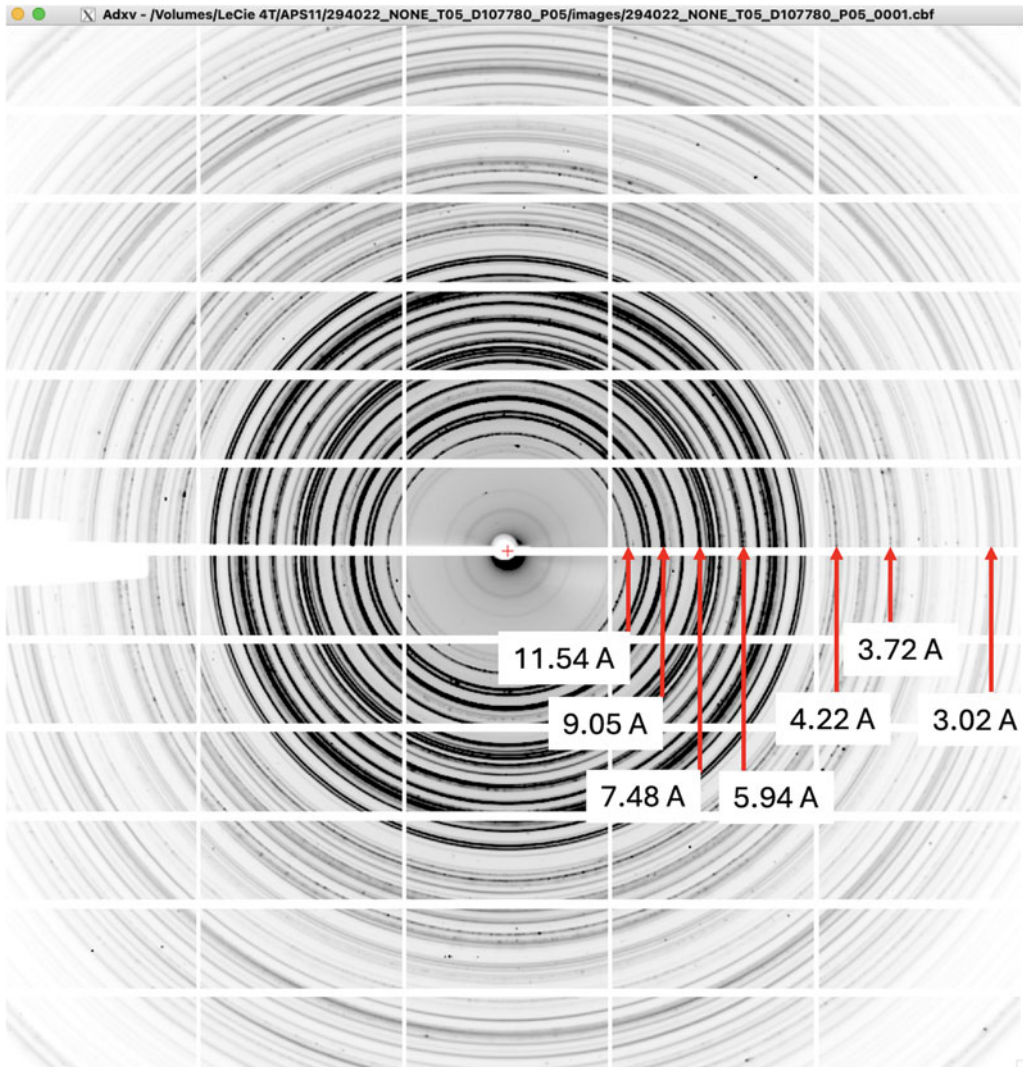
Figure 7. *X-ray diffraction at 2.066 Angstrom from ooid in present era stromatolite showing dark lattice rings between 11.54 and 4.81 Angstroms from the centre outward, plus rings including calcium carbonate in the outer faint pattern.*

The results of this whole scan are plotted in Fig. S2.3 with the most prominent clusters listed here in Table 4. Long sequences of higher order matches prompted the next stage of analysis in which the higher order fits were compared to '*D*' spacing expectations for the putative diamond 2H lattice (McGeoch *et al.*, 2021) of hemoglycin, the detailed calculation of these spacings being laid out in S2. Initially, with undistorted perfectly tetrahedral lattice vertices there was moderately good agreement, however excellent agreement was obtained with a 4.5 degree increase (to $23.97 \pm 0.5°$) in the angle α between the quasi-hexagonal 'sides' and the plane perpendicular to the trigonal symmetry axis (McGeoch *et al.*, 2021). It is concluded that the sample ooid from a recent stromatolite contains an axially distorted diamond 2H open 3D lattice with an inter-vertex spacing of 49.0 ± 0.2 Angstroms, and that iron atoms at the vertices provide the strong x ray scattering necessary to observe the lattice. The lattice is filled with calcium carbonate in the crystal forms aragonite and calcite. Because we see rings rather than spots, the ooid comprises a polymer lattice with multiple small crystals in many

Table 4 *Ooid diffraction rings in first order (left hand column). Higher order fits (top row) listed as diffraction order with percentage mis-match*

Angstroms	49.0	81.65	92.05	112.75	119.9	126.25
4.80(8)		17, 0.1%			25, 0.2%	
5.18(5)						
5.24(3)			17, 0.1%			24, 0.3%
5.44(5)	9, 0%	15, 0.2%			22, 0.1%	
5.63(3)				20, 0.1%		
5.73(5)					21, 0.4%	22, 0.1%
5.94(3)			15, 0.1%	19, 0.1%		
6.28(8)		13, 0.4%		18, 0.4%	19, 0.3%	20, 0.4%
6.57(8)						
6.84(5)			13, 0.1%			
7.02(2)	7, 0.3%			16, 0.3%	17, 0.4%	18, 0.1%
7.12(8)						
7.48(5)				15, 0.4%	16, 0.1%	
8.12(7)	6, 0.5%	10, 0.1%	11, 0.3%			
9.05(3)		9, 0.2%				14, 0.3%
9.82(3)	5, 0.2%					
10.21(7)		8, 0.1%		11, 0.3%		
11.54(0)						

orientations. The hemoglycin lattice itself is in many orientations, possibly aligned in regions associated with micro-crystals.

Additional first order diffraction data from crystals and ooids

In Section S3 additional diffraction data is given on (a) crystals in fossil stromatolite extract and (b) ooids from both present day and fossil stromatolite. Out of the fossil samples, only fossil No. 2 from Wyoming (provenance in Methods) yielded any ooids. X-ray diffraction results for ooids in the two present day stromatolites and in a second Wyoming sample, No. 2, are compared in Table S3.1. No ooids could be found in Fossil stromatolite No. 1.

In regard to (a): In Table S3.1 there was a degree of commonality between different crystal samples of Wyoming Fossil No. 1, and a match between fossil stromatolite and the prior report of diffraction from a fiber crystal of meteorite Acfer 086. The agreement related to the proposed separation of iron atoms at the junction of hemoglycin rods in a rectangular lattice (McGeoch and McGeoch, 2021).

In regard to (b): Table S3.2 compares ring patterns in ooids (provenance in Section S3.2). The Shark Bay ooids are 1. as found, and 2. acid treated as in Methods. The San Salvador ooids were the most recent. Many of the rings were identified as aragonite. Interestingly the 2.1 Gya fossil also contained aragonite, implying a 'mild' thermal history in view of the tendency for aragonite to transition into more stable calcite at high temperatures (Parker *et al*., 2010).

Section 4. Infrared absorbances of stromatolite ooid and meteoritic material.

Amide I components as an indicator of secondary structure

Hemoglycin, primarily composed of antiparallel strands of glycine, has the same peptide backbone as the synthetic polypeptide poly-L-lysine which has been extensively studied. Susi *et al*. (1967) reported infrared absorption measurements of the transition from random conformation through alpha-helix to

antiparallel-chain pleated beta sheet. For poly-L-lysine in the random configuration there was a single amide I band centred at 1647 cm^{-1} (6.07 μm) that was relatively broad at 40 cm^{-1}. After transition to an antiparallel beta sheet the amide I band was split into two components, the $a-$ at 1616 cm^{-1} (6.19 μm) and the $a+$ at 1690 cm^{-1} (5.92 μm) in the case of H$_2$O solution, each having a relatively narrow width of <20 cm^{-1}. In that work the related amide II band, typically seen at about 1550 cm^{-1} (6.45 μm), was suppressed by deuteration of the amide nitrogen (Blout *et al.*, 1961; Susi *et al.*, 1967) a consequence of D$_2$O being preferentially used (Susi *et al.*, 1967) in order to avoid H$_2$O absorption around 6 microns.

The degree of amide I splitting increases with the areal extent of the antiparallel beta sheet, details reported by Cheatum *et al.* (2004). In (Cheatum *et al.*, 2004, Fig. 4) it is found that the splitting is mostly accomplished at the scale of 4×4 unit cells in a model, where each unit cell covers four amino acid residues, two in one chain hydrogen-bonded to a pair in an adjacent antiparallel chain. The lower frequency peak $a-$, at 1635 cm^{-1} (6.12 μm) in Cheatum *et al.* (2004), is always much more intense than the up-shifted $a+$ peak at 1680 cm^{-1} (5.95 μm). This splitting does not occur at all in a two-strand antiparallel beta sheet, but always occurs in extended antiparallel beta sheets to the extent that numerous authors have identified the amide I splitting as a reliable marker for the antiparallel beta sheet secondary structure (Miyazawa, 1960; Miyazawa and Blout, 1961; Chirgadze and Nevskaya, 1976; Cheatum *et al.*, 2004). The calculated strength ratio (Chirgadze and Nevskaya, 1976) of $a+$ to $a-$ is low, as seen experimentally in poly-L-lysine (Demirdoven *et al.*, 2004) and again in the present data for hemoglycin.

Analysis of the infrared absorption
1. The amide bands (inset to Fig. 8) dominate the mid-IR absorption in both meteorite and ooid samples.
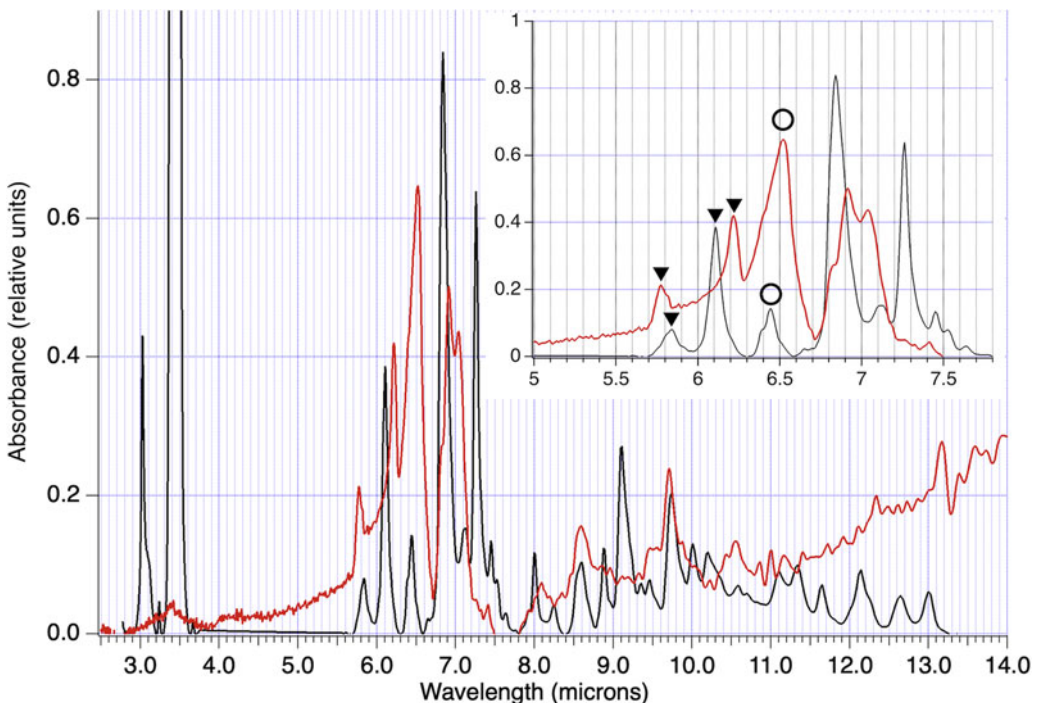

Figure 8. *Reproduced from (McGeoch and McGeoch, 2024, Fig. 3) Mid-infrared absorption spectra of Meteorite crystal SM2 (black lines) and Shark Bay stromatolite ooid (red lines). Inset: Amide I components filled triangles. Amide II components circles.*

2. Both samples show Amide I splitting into two components: a strong lower frequency component and a very much weaker higher frequency component. These are identified with the extensively researched $a-$ and $a+$ components, respectively. The degree of splitting depends upon the extent of the sheet and whether it has multiple layers. The SM2 crystal has less extensive sheets, correlated with less splitting. In support of this is the presence in SM2, but not in ooid, of a very strong 3300 cm^{-1} (3.03 μm) band due to N-H stretch, implying a large component of N-H groups that are freely vibrating as opposed to being involved in the C = O--H-N hydrogen bond within an extended sheet (Fig. S1.2 for illustration of N-H stretch and antiparallel beta sheet).

In view of the above we conclude that each of the substances under test is a polymer of amino acids arranged in an extended antiparallel beta sheet.

3. The amide II band is also seen in both samples, at 1534 cm^{-1} (6.52 μm, ooid) and 1550 cm^{-1} (6.45 μm, SM2 crystal). The Amide II band of hemoglycin in ooid is more intense than amide I, contrary to the observation in SM2 and to the approximately 0.5 ratio expected for amide II/amide I in an extended antiparallel beta sheet (Chirgadze and Nevskaya, 1976; Moore and Krimm, 1976). The reason for this anomalous Amide II intensity in ooid is not known.

In the ooid data of Fig. 8 the complex of bands between 6.8 and 7.1 μm (inset) is due to amorphous calcium carbonate (Avaro *et al.*, 2019), additionally identified by its diminution with longer acid treatment. In the same region the meteoritic spectrum has strong and relatively sharp absorptions at 1462 cm^{-1} (6.84 μm) and 1377 cm^{-1} (7.26 μm) that are not spatially correlated with the amide band absorptions within the crystal. They are from a non-amide source that has been identified (Tielens *et al.*, 1984) as most probably saturated hydrocarbons, the closest match being to pentane, which has CH$_2$ deformation bands at 1470 cm^{-1} (6.80 μm) and 1378 cm^{-1} (7.26 μm). Saturated hydrocarbons may constitute more than 30% of all the carbon in the line of sight to these protostar sources (Tielens *et al.*, 1984). We emphasize that hemoglycin in material ultimately derived from a molecular cloud has hydrocarbon bands that are known to be dominant in the interstellar medium (McGeoch and McGeoch, 2024) whereas the recent ooid FTIR had no hint of these saturated hydrocarbons.

Discussion

We find that four very different lines of evidence all point to the presence in stromatolites of the hemoglycin polymer previously only known from meteorites. In the first 2.1 Gya fossil stromatolite sample the fraction of heavy isotopes in the core unit mass spectrometry peak complex is comparable to that in the Orgueil meteorite, which seems to indicate that there was preservation of in-fall hemoglycin in the predominantly calcium carbonate fossil. Following studies of the Barberton Greenstone Belt of South Africa, Lowe and Byerly (2018) have discussed revision of the temporal profile of meteoritic in-fall towards an ongoing, more gradual decline (Neukum *et al.*, 2001) than in the Late Heavy Bombardment theory in which in-fall declined abruptly to present day levels at about 3.9 Gya. The in-fall rate at 2.5 Gya, the end of the Archean, may have been 10 times greater than at present. Most of the in-falling material would likely resemble the Orgueil meteorite, which is known to be characteristic of solar system material (Gounelle and Zolensky, 2014). Our present work with Orgueil has shown that relatively complex chemicals such as hemoglycin can survive in-fall, although not, presumably, in the heat and shock conditions of a major impact.

We estimate that the present-day rate of hemoglycin in-fall is of the correct order of magnitude to in principle create the internal organic lattice of recent ooids. Measurements of particles in Antarctic snow (Rojas *et al.*, 2021) confirm that sub-millimetre cosmic dust dominates present day in-fall, either as cosmic spherules or un-melted fine-grained material. Within the latter category, falling on Earth at a measured 1600 ± 500 tons per year, Rojas *et al.* (2021) infer the existence of 26 ± 16 tons per year of 'unaltered' carbon representing potentially intact organic molecules of likely cometary origin.

From its dominance in our organic meteoritic extracts we estimate that possibly 20% of the carbon in carbonaceous chondrites is bound in the polymer amide hemoglycin. The hemoglycin molecule contains 32% by weight of carbon in its 1638 Dalton lattice version McGeoch and McGeoch (2021), leading to an in-fall estimate of 1.1×10^{13} molecules per m^2 per year. Each molecule can build a lattice volume of $9.0 \times 10^{-26} \, m^3$ (McGeoch and McGeoch, 2021) and hence the hemoglycin in-fall in one year on $1 \, m^2$ can in principle build enough lattice to guide the crystallization of aragonite within one ooid of diameter 125 microns. It is possible that convection brings sufficient ocean-borne hemoglycin into shallow regions of high calcium carbonate to drive the steady formation of ooids over timescales of thousands of years. In this scenario the local rate of ooid formation would be constrained by the rate of hemoglycin in-fall combined with its transport to shallow shoals.

Calcium carbonate ooids are the primary mineral constituent of present-day stromatolites. However, through geological time there can be partial replacement of calcium carbonate in ooids by silicates, as seen by for example (Flannery *et al.*, 2019) in 2.72 Gya fossil ooids from Western Australia. In our X-ray study of 2.1 Gya fossil stromatolite the dominant crystal form is aragonite, indicating not only a mild thermal history, as discussed above, but minor aqueous alteration (Dravis and Yurewicz, 1985).

The survival of hemoglycin is attributed to its being an incredibly tough molecule, that, once formed in a protoplanetary disc, often becomes internally mineralized, remaining within the mineral as an extensive low-density lattice. This state has now been observed for the first time in our X-ray analysis at 2 Angstroms. In the protoplanetary disc, molecules circulate from hot, high ultraviolet, to cold regions and should an open hemoglycin lattice get near the new sun it would degrade and never feature as an in-fall polymer. Hemoglycin is found in many meteorites indicating that some hemoglycin from the colder regions of the disc does persist to seed planets via in-fall. Planets forming from a protoplanetary disc via gravity, as they enlarge, experience heating due to Al isotope decay, meaning that hemoglycin landing on such an early entity will not remain intact. A planet like Earth conducive to developing complex chemistry, going on to life forms, will rely on asteroid in-fall once it is sufficiently cool for the molecules to survive.

Beginning approximately 2.4 Gya and reaching partial completion 2 Gya, there was a build-up of oxygen in Earth's atmosphere from almost zero to a fraction of the present day value, known as the great oxygenation event (GOE) (Olejarz *et al.*, 2021). It has been proposed that gradually cyanobacteria dominated over anoxygenic photosynthetic bacteria, in a process dependent on geochemical changes together with locally increasing sources of oxygen (Olejarz *et al.*, 2021). However ultraviolet radiation reaching the Earth's surface prior to this event was as much as 400 times greater than in the present day (Cockell, 2000; Karam, 2003). This was in the UV band approximately between 200 nm and 300 nm which is the most destructive to nucleotides, equivalent to an E. Coli mutation doubling dose every quarter second (Cockell, 2000), much too high for any organism to survive. It requires several metres of water to attenuate the pre-GOE radiation levels to equate with present day surface exposure. The question is whether the earliest organisms were able to constitute themselves and thrive sufficiently to perform global oxidation in spite of an extremely hostile surface environment. Out of the present work comes an alternate hypothesis related to the possibility of reliable abiotic water splitting by hemoglycin in the presence of sunlight.

We have done initial quantum chemical modelling on a water-splitting reaction that hemoglycin can engage in, via direct absorption of UV light. We believe that it is a two-step reaction cycle that goes via

1. $hemoglycin + H_2O + h\nu \rightarrow hemoglycin \, (OH) + H_2$
2. $hemoglycin(OH) + H_2O + h\nu \rightarrow hemoglycin + H_2O_2$

followed by the release of O_2 from H_2O_2.

There are no other participants in this process, no catalysts and 'room temperature' operation. The finding of hemoglycin in a fossil stromatolite therefore opens up the possibility that its (proposed) oxygen producing ability could have 'kick-started' the GOE, producing an increasing degree of ultraviolet protection for complex biology. Furthermore, it could potentially provide chemical energy to its surroundings.

Here we assess that sufficient hemoglycin in-fall would have been available to in principle drive significant oxygenation of the atmosphere. We surmise that in its proposed water-splitting role hemoglycin would be attached within a 'platform' such as calcium carbonate crystals in shallow seas. The ultraviolet transmission of calcite is excellent and aragonite micro-crystals like those arranged within ooids (Simone, 1980) have a very large surface area for interaction with water. The photon efficiency is not known at present, but if we suppose that 0.1% of the incident pre-oxygenation solar spectrum at Earth's surface caused the two-step splitting reaction to occur, and that the in-fall rate for hemoglycin was ten times higher than today (discussed above), then a molecular coverage to support 0.1% absorption efficiency (10^{21} molecules m^{-2}) would be available in 10 My, and the entire oxygenation could be performed in less than 500My at a coverage of 10^{-5} of Earth's surface by ooid shoals. In this picture, the increasing ultraviolet absorption by oxygen and ozone in the atmosphere, combined with the decreasing rate of in-fall and the advent of bacterial films with ultraviolet absorption (DeCarvalho, 2017; Diaz and Eberli, 2019; Stolz, 2023), would put a cap on the attainable oxygenation level via hemoglycin. Oxygenation by cyanobacteria would continue, and in fact come to dominate.

The R-chirality of hemoglycin that lets it absorb visible light (McGeoch and McGeoch, 2022) sets it apart from S-based life involving amino acid protein. This may be its most important property allowing separation of systems with hemoglycin that are essentially abiotic to be very distinct from biochemical systems. On early Earth this system divide could have been maintained with fossil stromatolites forming their mineral parts abiotically (Grotzinger and Rothman, 1996; Trower et al., 2018), in possible contrast to present day stromatolites (Dupraz et al., 2009). However, there is evidence of organic material comparable to that in present day stromatolites having been present in the neo-Archean (Flannery et al., 2019). It would be of great interest to know whether hemoglycin present in modern day ooids still provides an energy source.

A 2023 report emphasizes that UV-driven chemistry in protoplanetary disks is a 'signpost' for planet formation (Calahan et al., 2023). The hemoglycin polymer is not referenced in Calahan et al. (2023) with its response at both 480 and 6 μm (McGeoch and McGeoch, 2022; 2024) but at least the factor of light on molecules is raised. In McGeoch and McGeoch (2022, 2024) we suggested that hemoglycin was a factor in accretion. To acknowledge the need for an abiotic factor, in this case light, acting on a molecule that allows energy transfer is a step forward to understanding paths to the evolution of accreted matter destined for planet formation and for biochemical evolution. In McGeoch and McGeoch (2024) it was proposed that hemoglycin is a molecular candidate for absorption in molecular clouds from 3–13.2 microns with strong peaks at 6.2 microns.

In McGeoch and McGeoch (2021, 2022, 2024) our observations pointed to hemoglycin potentially being an accretor molecule, in Space or on Earth, by virtue of its open 3D lattice which can accommodate different minerals or molecular types. In (McGeoch and McGeoch, 2021) we found that the diamond-2H 3D lattice of hemoglycin was able to expand into the largest volume using the least length of polymer. Supposing that an anti-parallel chain of glycine constituted the most rigid, yet lightweight rod-like molecular form, then hemoglycin would be the most efficient available molecule to aid ooid formation by lattice extension followed by internal aragonite crystallization.

Conclusions

Modern day stromatolite ooids and fossil stromatolite (2.1 Gya) from the Medicine Bow Mountains of Wyoming contain hemoglycin, the space polymer. At 2.1 Gya there was ongoing substantial asteroidal delivery, including hemoglycin, to Earth where water was present as tidal pools or early oceans, conditions that support stromatolite formation. Light is the important agent for hemoglycin in that it allows the molecule to potentially pass on energy to other chemistry, and possibly lead to atmospheric oxidation. Once the early Earth had hemoglycin it had solar driven chemical energy that may have led by paths unknown and to be investigated, to the first life forms, the stromatolites and their bacterial mats. The first events together (hemoglycin in-fall and formation of first stromatolites) could have been abiotic and may have preceded simple organisms like cyanobacteria.

References

Avaro JT, Ruiz-Agudo C, Landwehr CE, Hauser K and Gebauer D (2019) Impurity-free amorphous calcium carbonate, a preferential material for pharmaceutical and medical applications. *European Journal of Mineralogy* **31**, 231–236.

Bekker A and Eriksson KA (2003) A paleoproterozoic drowned carbonate platform on the southeastern margin of the Wyoming Craton: a record of the Kenorland breakup. *Precambrian Research* **120**, 327–364, and D. Lageson, private communication.

Berman A, Hanson J, Leiserowitz L, Koerzle TF, Weiner S and Addadi L (1993) Biological control of crystal texture: A widespread strategy for adapting crystal properties to function. *Science (New York, N.Y.)* **259**, 776–779.

Blout ER, De Loze C and Asadourian A (1961) The deuterium exchange of water-soluble polypeptides and proteins as measured by infrared spectroscopy. *Journal of the American Chemical Society* **83**, 1895–1900.

Calahan JK, Bergin EA, Bosman AD, Rich EA, Andrews SM, Bergner JB, Cleeves LI, Guzman VV, Huang J, Ilee JD, Law CJ, Le Gal R, Oberg KI, Teague R, Walsh C, Wilner DJ and Zhang K (2023) UV-driven chemistry as a signpost of late-stage planet formation. *Nature Astronomy* **7**, 49–56.

Cheatum CM, Tokmakoff A and Knoester J (2004) Signatures of beta-sheet secondary structures in linear and two-dimensional infrared spectroscopy. *Journal of Chemical Physics* **120**, 8201–8215.

Chirgadze YN and Nevskaya NA (1976) Infrared spectra and resonance interaction of amide-I vibration of the antiparallel-chain pleated sheet. *Biopolymers* **15**, 607–625.

Cockell CS (2000) The ultraviolet history of the terrestrial planets – implications for biological evolution. *Planetary and Space Science* **48**, 203–214.

DeCarvalho CCCR (2017) Biofilms: microbial strategies for surviving UV exposure. Chapter 19 *Ultraviolet Light in Human Health, Diseases and Environment. Advances in Experimental Medicine and Biology* **996**, 233–239.

Demirdoven N, Cheatum CM, Chung HS, Khalil M, Knoester J and Tokmakoff A (2004) Two-dimensional infrared spectroscopy of antiparallel beta-sheet secondary structure. *Journal of the American Chemical Society* **126**, 7981–7990.

Diaz MR and Eberli GP (2019) Decoding the mechanism of formation in marine ooids: A review. *Earth-Science Reviews* **190**, 536–556.

Dravis JJ and Yurewicz DA (1985) Enhanced carbonate petrography using fluorescence microscopy. *Journal of Sedimentary Petrology* **55**, 795–804.

Dupraz C, Reid RP, Braissant O, Decho AW, Norman RS and Visscher PT (2009) Processes of carbonate precipitation in modern microbial mats. *Earth-Science Reviews* **96**, 141–162.

Flannery DT, Allwood AC, Hodyss R, Summons RE, Tuite M, Walter MR and Williford KH (2019) Microbially influenced formation of Neoarchean ooids. *Geobiology* **17**, 151–160.

Gounelle M and Zolensky M (2014) The Orgueil meteorite: 150 years of history. *Meteoritics & Planetary Science* **49**, 1769–1794.

Grotzinger JP and Rothman DH (1996) An abiotic model for stromatolite morphogenesis. *Nature* **383**, 424–435, (Cowles Lake Formation, Wopmay orogen, northwest Canada, age 1.9Gya).

IAEA, Vienna (1995) https://www.iaea.org/publications/4755/iaea-yearbook-1995

Karam PA (2003) Inconstant Sun: How solar evolution has affected cosmic and ultraviolet radiation exposure over the history of life on Earth. *Health Physics* **84**, 322–333.

Knoll AH (2012) Chapter 16 *The Fossil Record of Microbial Life* Editor(s): Andrew H. Knoll, Donald E. Canfield, Kurt O. Konhauser First published: 30 March (2012). doi: 10.1002/9781118280874.ch16

Lin Y, Power IM and Chen W (2022) Holocene lacustrine abiotic aragonitic ooids from the Western Qaidam Basin, Qinghai-Tibetan Plateau. *Minerals* **12**, 1400.

Lowe DR and Byerly GR (2018) The terrestrial record of Late Heavy Bombardment. *New Astronomy Reviews* **81**, 39–61.

Lu I-C, Chu KY, Lin CY, Wu SY, Dyakov YA, Chen J-L, *et al.* (2015) Ion-to-neutral ratios and thermal proton transfer in matrix-assisted laser desorption/ionization. *Journal of the American Society for Mass Spectrometry* **26**, 1242–1251.

McGeoch JEM and McGeoch MW (2015) Polymer amide in the Allende and Murchison meteorites. *Meteorit and Planet Science* **50**, 1971–1983.

McGeoch JEM and McGeoch MW (2021) Structural organization of space polymers. *Physics of Fluids* **33**, 067118.

McGeoch JEM and McGeoch MW (2022) Chiral 480 nm absorption in the hemoglycin space polymer: a possible link to replication. *Scientific Reports* **12**, 16198.

McGeoch JEM and McGeoch MW (2024), Polymer amide as a source of the cosmic 6.2 micron emission and absorption. *arXiv:2309.14914* [astro-ph.GA]. Mon. Not. Roy. Astr. Soc. doi: 10.1093/mnras/stae756.

McGeoch MW, Dikler S and McGeoch JEM (2021) Meteoritic proteins with glycine, iron and lithium, *arXiv:2102.10700*.

McGeoch MW, Owen RL, Jaho S and McGeoch JEM (2023a) Hemoglycin visible fluorescence induced by X rays. *Journal of Chemical Physics* **158**, 114901.

McGeoch MW, Samoril T, Zapotok D and McGeoch JEM (2023b) Polymer amide as a carrier of ^{15}N in Allende and Acfer 086 meteorites. Under review at *International Journal of Astrobiology*. https://arxiv.org/abs/1811.06578

Miyazawa T (1960) Perturbation treatment of the characteristic vibrations of polypeptide chains in various configurations. *Journal of Chemical Physics* **32**, 1647–1652.

Miyazawa T and Blout ER (1961) The infrared spectra of polypeptides in various conformations: amide I and amide II bands. *Journal of the American Chemical Society* **83**, 712–719.

Moore WH and Krimm S (1976) Vibrational analysis of peptides, polypeptides and proteins I. Polyglycine I. *Biopolymers* **15**, 2439–2464.

Neukum G, Ivanov BA and Hartmann W (2001) Cratering records in the inner Solar System in relation to the lunar reference system. *Space Science Reviews* **96**, 55–86.

Olejarz J, Iwasa Y, Knoll AH and Nowak MA (2021) The Great Oxygenation Event as a consequence of ecological dynamics modulated by planetary change. *Nature Communications* **12**, 3985.

Orgueil meteorite (n.d.) https://www.lpi.usra.edu/meteor/metbull.php?code=18026

Parker JE, Thompson SP, Lennie AR, Potter J and Tang CC (2010) A study of the aragonite-calcite transformation using Raman spectroscopy, synchrotron powder diffraction and scanning electron microscopy. *Crystal Engineering Communications* **12**, 1590–1599.

Paterson DM, Aspden RJ, Visscher PT, Consalvey M, Andres MS, Decho AW, Stolz J and Reid RP (2008) Light-dependent biostabilization of sediments by stromatolite assemblages. *PLoS One* **3**, e3176.

Pokroy B, Quintana JP, Caspi EN, Berner A and Zolotoyabko E (2004) Anisotropic lattice distortions in biogenic aragonite. *Nature Materials* **3**, 900–902.

Rojas J, Duprat J, Engrand C, Dartois E, Delauche L, Godard M, Gounelle M, Carillo-Sanchez JD, Pokorny P and Plane JMC (2021) The micrometeorite flux at Dome C (Antarctica), monitoring the accretion of extraterrestrial dust on Earth. *Earth and Planetary Science Letters* **560**, 116794.

Simone L (1980) Ooids: a review. *Earth-Science Reviews* **16**, 319–355.

Stolz JF (2023) Stromatolites: Linking the past to the future. *Environmental Microbiology* **25**, 158–160.

Sutter's Mill meteorite (n.d.) https://www.lpi.usra.edu/meteor/metbull.php

Susi H, Timasheff SN and Stevens L (1967) Infrared spectra and protein conformations in aqueous solutions. *Journal of Biological Chemistry* **242**, 5460–5466.

Tielens AGGM, Allamandola LJ, Bregman J, Goebel J, D'Hendecourt LB and Witteborn FC (1984) Absorption features in the 5–8 micron spectra of protostars. *The Astrophysical Journal* **287**, 697–706.

Trower EJ, Cantine MD, Gomez ML, Grotzinger JP, Knoll AH, Lamb MP, Lingappa U, O'Reilly SS, Present TM, Stein N, Strauss JV and Fischer WW (2018) Active ooid growth driven by sediment transport in a high-energy shoal, Little Ambergris Cay, Turks and Caicos islands. *Journal of Sedimentary Research* **88**, 1132–1151.